NMR IN BIOMEDICINE
NMR Biomed. 2007; **20**: 383–391
Published online in Wiley InterScience
(www.interscience.wiley.com) DOI:10.1002/nbm.1124

Measurement of nonlinear pO_2 decay in mouse lungs using ^{3}He-MRI

Katarzyna Cieślar,[1] Hasan Alsaid,[2] Vasile Stupar,[2] Sophie Gaillard,[2] Emmanuelle Canet-Soulas,[2] Rachida Fissoune[2] and Yannick Crémillieux[2]*

[1]Institute of Physics, Jagiellonian University, Kraków, Poland
[2]Université Lyon 1, Laboratoire de RMN, CNRS, CPE, Lyon, France

Received 14 June 2006; Revised 14 September 2006; Accepted 24 October 2006

ABSTRACT: Spatial and temporal variations in oxygen partial pressure (pO_2) during breath-hold can be exploited to obtain important regional parameters of lung function. In the course of apnea, the oxygen concentration is known to decay exponentially. Therefore, the initial pO_2 (p_0) can be used to represent local ventilation, and the oxygen depletion time constant can characterize perfusion. The protocol, based on a nonlinear model of pO_2 decay, was validated in six healthy mice. Parametric maps of p_0 and oxygen depletion time constant were obtained for pure ^{3}He and ^{3}He/air mixture. The mean measured values of p_0 were 77 ± 9 mbar for the pure ^{3}He insufflation and 107 ± 5 mbar for ^{3}He/air mixture, in agreement with the predefined p_0 values: 75 ± 15 mbar and 123 ± 15 mbar, respectively. The mean measured oxygen depletion time constants were 6.5 ± 0.2 s for pure ^{3}He and 7.1 ± 0.8 s for the ^{3}He/air mixture, in agreement with physiology.

KEYWORDS: hyperpolarized ^{3}He; oxygen partial pressure; oxygen uptake; lung function imaging; lung MRI

INTRODUCTION

The partial pressure of oxygen (pO_2) and its depletion rate are important parameters in lung function assessment. Alveolar pO_2 can be used as a marker of ventilation efficiency, and the oxygen depletion rate, which is related to oxygen uptake, can be used to characterize perfusion. It has been shown that measuring the time evolution of pO_2 enables differentiation between normal and diseased lungs in pulmonary embolism (1,2), obliterative bronchiolitis (3), sickle cell disease (4) and chronic obstructive pulmonary disease (5). Previously reported pO_2 measurements in both animals (1,2,6–15) and human subjects (3,4,6,10,16–18) were restricted to short breath-hold periods when a linear model of pO_2 decrease can be assumed in the form:

$$pO_2 = p_0 - Rt$$

where p_0 is the initial pO_2 and R is related to oxygen uptake into the blood.

Rodents are often used for studying disease development and following treatment involving new drugs. There is a large number of available transgenic mouse models for a variety of ailments affecting man. However, the high metabolic rate of mice results in very fast pO_2 decay times of the order of a few seconds. Therefore, it is necessary to study oxygen decay dynamics without using the simplified model of linear decrease in pO_2.

As the oxygen concentration in the lungs during apnea is known to decrease exponentially (19), we proposed the use of a more general model of pO_2 decay in the form:

$$pO_2 = p_0 \exp(-t/r)$$

where p_0 is the initial pO_2 and r is the oxygen depletion time constant. We present the parametric maps of p_0 and r obtained for six healthy mice using this novel approach. To be able to follow rapid changes in pO_2, the fast spiral single-breath method with a sliding window technique for RF correction was exploited.

MATERIALS AND METHODS

Acquisition sequence

Of all the factors that influence the ^{3}He signal in the lungs, RF excitation and the presence of paramagnetic oxygen are the dominant depolarization effects (6). To separate these two factors, a single-acquisition pO_2-sensitive technique based on spiral sampling was developed.

A single experiment consisted of a series of N images separated by a user-defined delay time τ, except the first

*Correspondence to: Y. Crémillieux, Laboratoire de RMN, ESCPE, 43 Boulevard du 11 Novembre, 69622 Villeurbanne Cedex, France.
E-mail: yannick.cremillieux@univ-lyon1.fr
Contract/grant sponsor: French CNRS-CEA "Small Animal Imaging" Program, and an MIRA grant from the Rhône-Alpes Region.

Abbreviations used: FRC, functional residual capacity; pO_2, partial pressure of oxygen; ROI, region of interest; SNR, signal-to-noise ratio.

two images which were acquired without any delay (Fig. 1a). The delay, τ, was chosen individually for each acquisition, depending on the expected $T_{1,O2}$ relaxation time. For all of the *in vivo* experiments, the shortest possible τ was used, equal to 527 ms. In the case of *in vitro* experiments, the delay time was varied between 1.3 s and 30.3 s. Acquisition with 12 interleaved Archimedean spirals per image (20) was used with the following imaging parameters: 1024 samples per spiral, flip angle $\alpha \approx 6^\circ$, $TE = 2$ ms, $TR = 27.3$ ms, field of view = 40 mm, and slice thickness = 60 mm (projection images). The flip angle was calibrated on a helium-filled syringe by measuring the signal decay due to a train of quickly repeated RF pulses. The first two sets from each series were later reconstructed using the sliding window technique (21,22), which is based on shifting the reconstruction window along the two data sets so that each consecutive image contains 12 spirals (Fig. 1b). As a result of this procedure, 13 images were reconstructed with the delay time of one *TR* (27.3 ms) and with only one RF excitation between consecutive images. This allows the map of the RF flip angle of the object to be obtained on a pixel-by-pixel basis. After RF correction, the series of *N* images was used to determine the time dependence of pO_2.

Experimental protocol

The experiments were performed on a 2 T magnet (Oxford Instruments, Oxford, UK) interfaced with the MRRS console (Guildford, UK). For gas polarization, a home-built spin-exchange polarizer was used (23,24). *In vitro* experiments were performed on a syringe filled with mixtures of ^{3}He and air with delay time, τ, of 1.3–30.3 s depending on the mixture composition. With local ethics committee approval, six female c57BL/6 mice (body weight 22–26 g, mean 24 g) were anesthetized by intraperitoneal injection of sodium pentobarbital, and tracheotomized. The animals were placed supine in an Alderman-Grant coil inside the magnet, and their lungs were insufflated with 0.8 ml gas. Each animal underwent four consecutive inhalations separated by appropriate delays to allow the normal oxygen concentration in the lungs to be restored. The first two insufflations were performed with 0.8 ml pure ^{3}He, and the other two with 0.5 ml ^{3}He mixed with 0.3 ml air. The gases were premixed in a syringe and immediately administered through the endotracheal tube into the mouse lungs. During the following breath-hold, a series of 12 projection images was acquired with delay time $\tau = 527$ ms between consecutive images (total acquisition

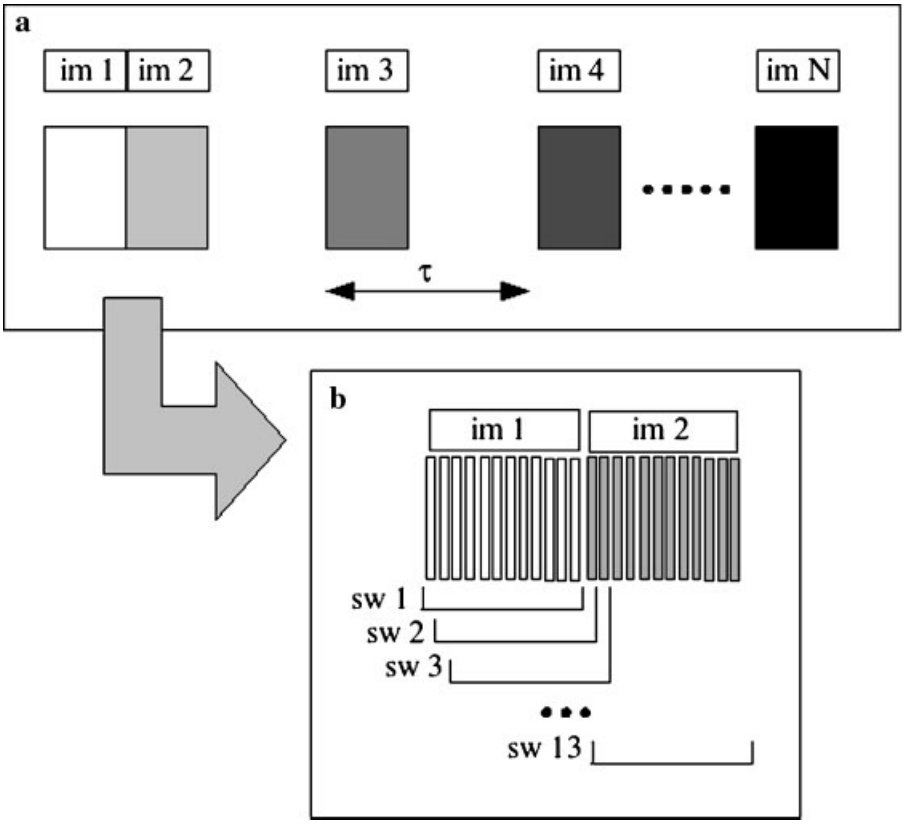

Figure 1. Schematic of the acquisition sequence (a) with sliding window diagram (b). Each image consists of 12 interleaved spirals. im, Image; sw, sliding window image.

DOI: 10.1002/nbm

time 5.6 s). Insufflation with pure ^{3}He was performed to assess the residual oxygen content in the functional residual capacity (FRC) of the animal's lungs. The purpose of repeating the experiment with the same gas composition was to obtain both transverse and coronal projection series.

Image reconstruction and analysis

For image reconstruction and processing, software written in IDL (RSI; Boulder, CO, USA) was developed. Spiral images of matrix size 256×256 were reconstructed using a gridding algorithm (25,26). Two user-defined regions of interest (ROIs), one selected within the imaged object and the second in the background, served to estimate the signal-to-noise ratio (SNR) and the standard deviation of noise σ. The signal in each pixel was then corrected for noise according to the scheme proposed by Gudbjartsson and Patz (27). Finally, the images were masked so that only pixels with signal above a predefined threshold were used in further analysis. The threshold was calculated individually for each image series and was based on the noise level of the first image according to:

$$\text{Threshold} = \text{Mean noise figure} + 3\sigma \qquad (1)$$

From the first two images in each series, 13 images were reconstructed using the sliding window technique, and a map of RF flip angle was constructed on a pixel-by-pixel basis (128×128). Assuming $\alpha = 6^\circ$, $p_0 = 100$ mbar, $r = 6$ s, the overall decrease in signal due to both RF excitation and the presence of O_2 during the acquisition of the first two images (655 ms) is of the order of 15%, of which the RF contribution exceeds the pO_2 component sevenfold. Therefore, neglecting the pO_2 relaxation effect during the acquisition of the first two images, signal decay due to RF excitation alone is given by:

$$S(n) = S(0)\cos^n(\alpha) \qquad (2)$$

where $S(n)$ is the signal intensity in the nth image of the sliding window series, and α is the flip angle.

Fitting $\ln(S)$ against the sliding window image number n gives the value of the flip angle for every pixel of the image, providing the flip angle map of the imaged object. The RF correction was performed on a pixel-by-pixel basis by dividing the signal in each consecutive image in the series by the term $\cos^{12m}\alpha$, where α is the flip angle in a particular pixel and m is the image number.

After the flip angle correction, the actual pO_2 measurement was performed. As described by Deninger *et al*. (6,7), the signal intensity S_m in the series of m images can be expressed in the following way:

$$S_m = S_0 \exp[-\xi^{-1} \int_0^{m\tau} pO_2(t')dt'] \qquad (3)$$

where $\xi = 2.6$ (bar $\times$ s) at body temperature (28).

Assuming the decrease in pO_2 in the form:

$$pO_2 = p_0 \exp(-t/r) \qquad (4)$$

the time of evolution of the integral of pO_2 can be extracted from:

$$-\xi[\ln(S_m/S_0)] = \int_0^{m\tau} pO_2(t')dt' = \int_0^{m\tau} p_0 \exp(t'/r)dt' \qquad (5)$$

which can be evaluated as follows:

$$-\xi[\ln(S_m/S_0)] = p_0 r[1 - \exp(-t/r)] \qquad (6)$$

where $t = m\tau$.

Fitting the data with the expression on the right side of eqn (6) gives the p_0 and r values in each pixel.

Figure 2 illustrates the basic idea of the theoretical approach outlined above. The theoretical temporal evolution of the pO_2 integral is plotted for different p_0 and r values. In the case of no oxygen uptake ($r = \infty$), the pO_2 integral increases linearly (Fig. 2a), while significant deviation from linearity is observed for $r = 6$ s, expected *in vivo* (29–31). Varying the initial pO_2 at constant r changes the curve saturation level as shown in Fig. 2(b).

For calculation of the p_0 and r maps, a grid of 64×64 was imposed on the RF-corrected images, resulting in a bin size of 1.6 mm^2. In addition to computing the parametric maps (RF flip angle, p_0 and r), the processing procedure enables user-selected ROI analysis. ROIs of any shape and size for local pO_2 measurement can be chosen manually in different parts of the lungs. The mean signal in the ROI is then processed in the same manner as described above for each bin.

The *in vitro* experiments were performed in a syringe with predefined ^{3}He/air mixtures. Therefore, constant $pO_2(t) = p_0$ was assumed, and the appropriate integral in the form $\int_0^{m\tau} pO_2(t')dt' = p_0 t$ was fitted to the data.

Simulation

To investigate the influence of the SNR on the accuracy of the pO_2 measurement, a simulation program written in IDL was developed. For this purpose, a reference spiral image was acquired on a ^{3}He-filled syringe phantom. A series of copies of this data set was produced, and the signal decay was simulated assuming an exponential pO_2 decay model with the following parameters: $p_0 = 100$ mbar, $r = 6$ s, number of images = 12, corresponding to the experimental conditions. Each individual spiral was weighted according to eqn (3) and followed by image reconstruction. The SNR of the image was varied by the addition of artificially generated Gaussian noise. The parametric maps of p_0 and r were generated for each SNR value ranging from 23 to 120, and the mean p_0 and r

DOI: 10.1002/nbm

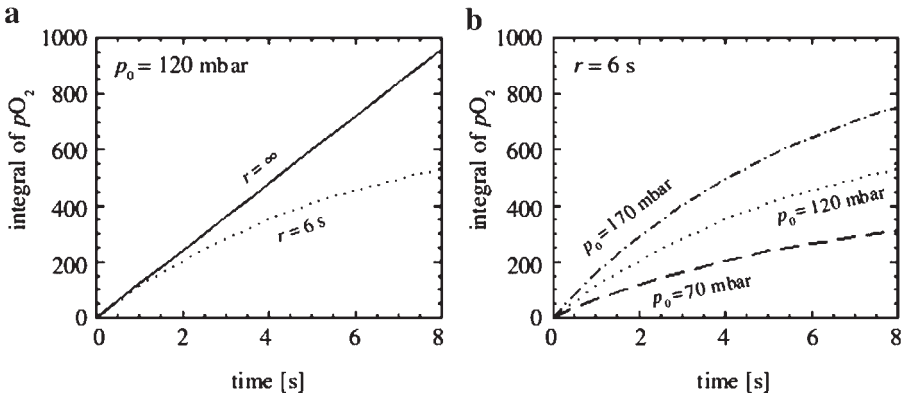

Figure 2. Theoretical plots of the temporal evolution of the pO_2 integral for different p_0 and r values. (a) Comparison of the plots for constant $p_0 = 120$ mbar with ($r = 6$ s) and without oxygen uptake ($r = \infty$). (b) Comparison of plots for different physiological p_0 values (70, 120, 170 mbar) at constant r (6 s).

values together with their standard deviations were computed.

RESULTS

In vitro experiments

In order to verify the accuracy of the proposed pO_2-sensitive technique, *in vitro* acquisitions were performed on a plastic syringe filled with pure ^{3}He and different ^{3}He/air mixtures (3.5, 4.5 and 6.0 ml air mixed with 5 ml ^{3}He). For each experiment, 5 ml ^{3}He was drawn from a storage syringe into a 10 ml probe syringe. In the case of experiments with ^{3}He/air mixtures, the probe was connected through a valve to an air-filled syringe from which an appropriate volume of gas was taken. The mixing was performed at ambient pressure, and, as a result, the total volume of the gas mixture was not constant. The mean measured p_0 values were 12, 83, 105 and 114 mbar corresponding to the expected values of 0, 88, 101 and 116 mbar, respectively. A comparison of the estimated ($p_{0,E}$) and the measured initial pO_2 values ($p_{0,M}$) is presented in Fig. 3. The uncertainties of $p_{0,E}$ were calculated on the basis of the dead volume of the valve (0.25 ml) and the mixing precision. The $\Delta p_{0,M}$ values are the standard deviation errors of the mean $p_{0,M}$ calculated over the whole map. The linear fit in the form $p_{0,M} = a + b p_{0,E}$ yielded: $a = 12.0 \pm 2.5$ mbar, and $b = 0.87 \pm 0.25$.

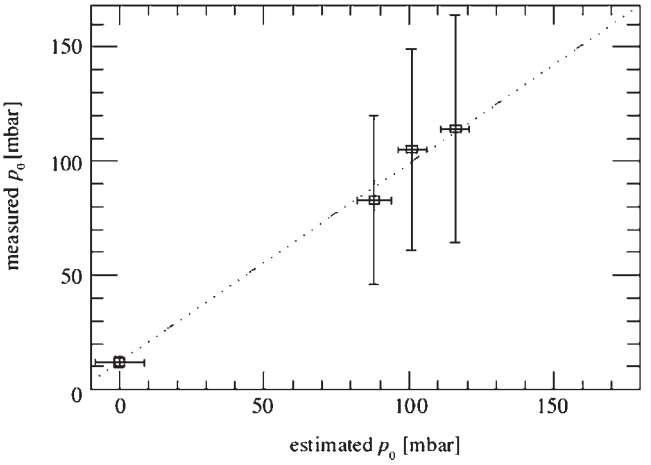

Figure 3. Comparison of the estimated and measured p_0 values *in vitro*. The dashed line shows the linear fit to the data, with the slope equal to 0.87 ± 0.25 and intercept of 12.0 ± 2.5 mbar.

In vivo experiments

The pO_2 measurements were carried out using pure ^{3}He (0.8 ml) and ^{3}He/air mixture (5.0 ml/3.0 ml). For each mouse, a series of images of lungs filled with pure ^{3}He was obtained in coronal and transverse orientation (Fig. 4), as well as transverse and coronal series of images for the ^{3}He/air mixture. The correction of the depolarization effect due to RF excitation was performed on the basis of the flip angle map calculated for each acquisition (Fig. 5). After the correction, the parametric maps of initial partial pressure of oxygen (p_0) and the depletion rate time constant (r) were computed for both types of inhaled gas composition (Fig. 6). Mean p_0 and r values together with their standard deviations were evaluated (Table 1). Out of the two acquisitions performed for each animal and each gas composition (in the coronal and the transverse orientation), the image series with higher initial SNR of the two was chosen for parametric mapping. The p_0 and r values for each pixel of the image were obtained by fitting the time evolution of the integral of pO_2 according to eqn (6) (Fig. 7a). To prove the

DOI: 10.1002/nbm

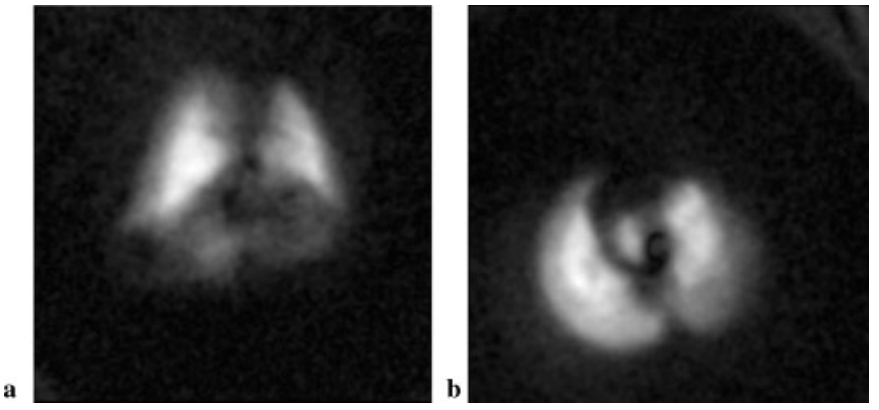

Figure 4. Native coronal (a) and transverse (b) images of mouse lungs (field of view = 40 mm; slice thickness = 60 mm).

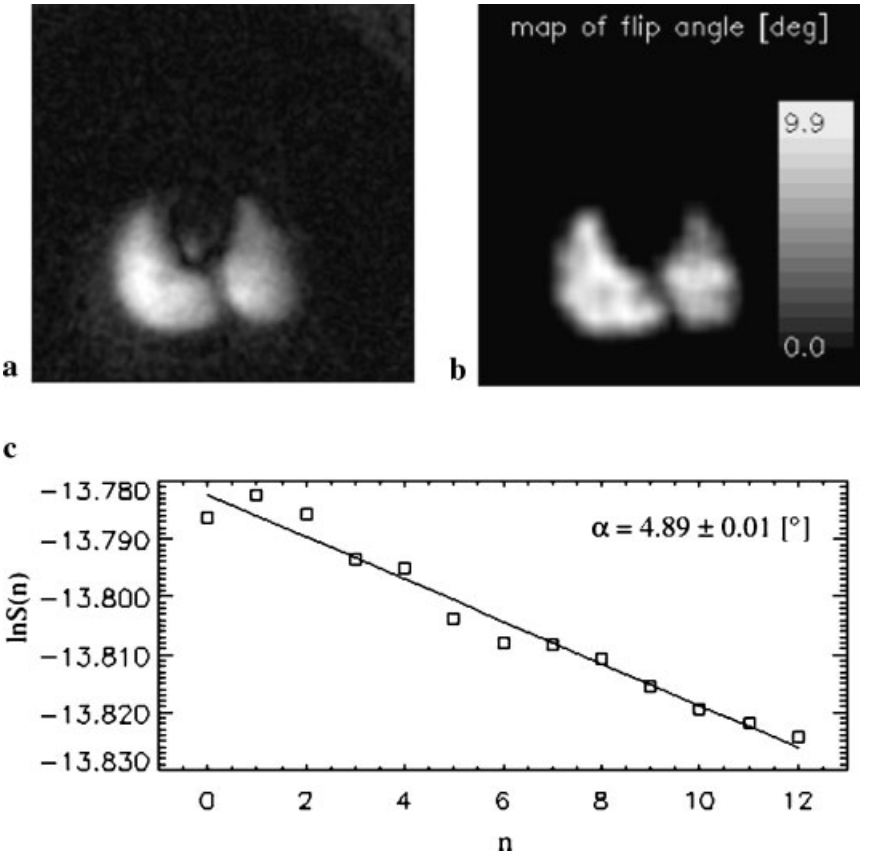

Figure 5. *In vivo* pure ^{3}He image (a) and the corresponding RF flip angle map (b). The mean flip angle was $4.3 \pm 1.1°$. (c) A typical plot used for RF flip angle estimation for one particular pixel; *n* denotes the sliding window image number [eqn (2)].

relevance of using the exponential model of pO_2 decay for data analysis, a comparison plot from the same ROI using the linear model is shown (Fig. 7b). The linear fitting was performed by the method proposed by Deninger *et al.* (6,7). Table 1 also contains the estimation of the linear oxygen depletion rate, *R*, for each acquisition (for details see Discussion).

Simulation results

The simulation was performed to investigate the effect of gradually increased noise in the image on the sensitivity of the proposed measurement technique. Figures 8 and 9 present the results of the simulation for p_0 and r, respectively. It can be seen that, regardless of SNR, the p_0

DOI: 10.1002/nbm

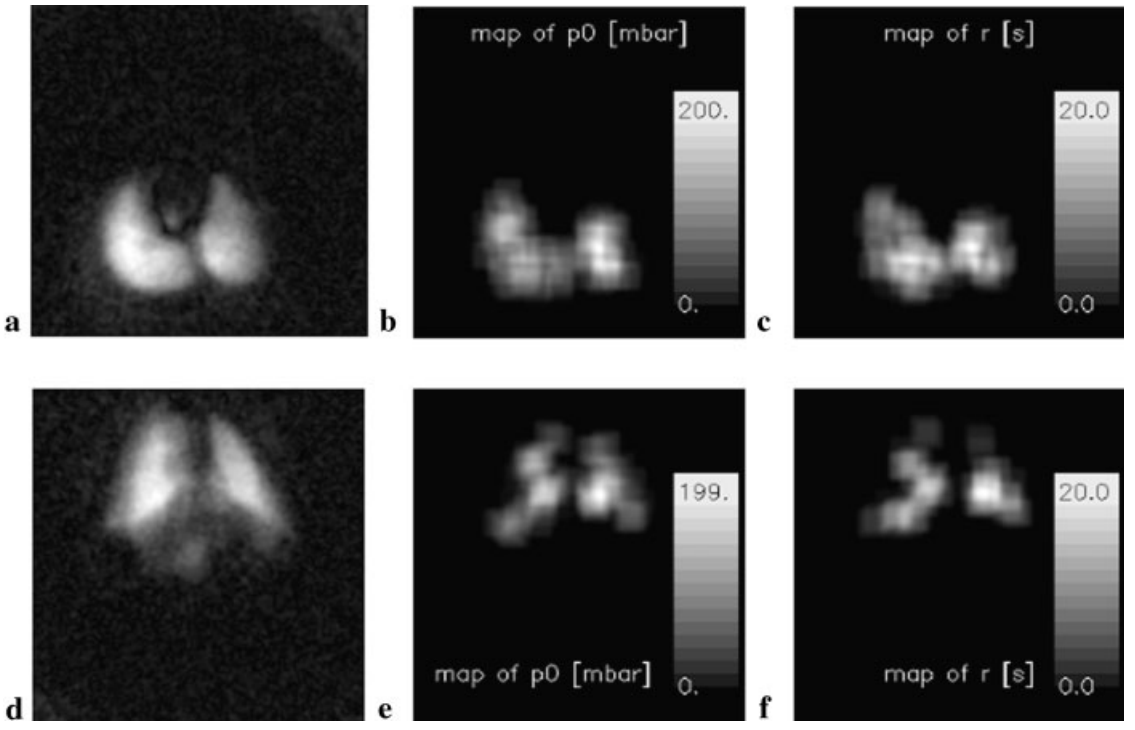

Figure 6. Exemplary results of insufflations with ^{3}He/air mixture (a–c) and pure ^{3}He (d–f). The initial images from each series are presented (a,d) together with corresponding p_0 maps (b,e) and r maps (c,f). Mean parameter values are: $p_0 = 112 \pm 59$ mbar, $r = 6.6 \pm 4.4$ s for ^{3}He/air mixture; $p_0 = 84 \pm 43$ mbar, $r = 6.4 \pm 4.6$ s for pure ^{3}He.

Table 1. Summary of RF flip angle, p_0 and r mapping. The measured values are given as mean ± sd

	Mouse 1	Mouse 2	Mouse 3	Mouse 4	Mouse 5	Mouse 6
Pure helium (expected p_0 value = 75 ± 15 mbar)						
SNR	103	92	69	118	121	93
α (°)	4.3 ± 1.1	5.1 ± 1.5	4.5 ± 1.6	5.9 ± 1.6	6.1 ± 2.0	6.1 ± 2.0
p_0 (mbar)[a]	64 ± 40	86 ± 52	84 ± 43	76 ± 45	68 ± 48	85 ± 40
r (s)	6.6 ± 4.1	6.8 ± 4.8	6.4 ± 4.6	6.5 ± 3.7	6.2 ± 5.0	6.2 ± 5.0
R (mbar/s)[b]	9.7 ± 8.5	12.6 ± 11.7	13.1 ± 11.6	11.7 ± 9.6	11.0 ± 11.8	13.7 ± 12.8
Mean measured $p_0 = 77 \pm 9$ mbar, $r = 6.5 \pm 0.2$ s						
Helium/air mixture (expected p_0 value = 123 ± 15 mbar)						
SNR	74	32	43	46	41	25
α (°)	5.9 ± 1.4	6.3 ± 1.7	6.3 ± 1.9	6.1 ± 1.9	6.6 ± 2.1	6.3 ± 2.3
p_0 (mbar)[a]	112 ± 59	99 ± 55	107 ± 58	108 ± 50	102 ± 38	111 ± 50
r (s)	6.6 ± 4.4	7.1 ± 5.2	8.3 ± 4.7	6.7 ± 4.8	7.7 ± 2.9	6.0 ± 5.2
R (mbar/s)[b]	17.0 ± 14.4	13.9 ± 12.8	12.9 ± 10.1	16.1 ± 13.7	13.2 ± 7.0	18.5 ± 18.1
Mean measured $p_0 = 107 \pm 5$ mbar, $r = 7.1 \pm 0.8$ s						

[a]Based on the gas mixture composition and the animal's FRC, assuming $[O_2] = 15\%$ in the FRC of the mouse lungs.
[b]Computed as the ratio of the mean values of p_0 and r.

values are systematically underestimated (by approximately 5%), and the r values are overestimated by about the same amount. Although the accuracy of the p_0 and r measurement is good, the precision is low, especially in the case of r determination.

DISCUSSION

The purpose of this study was to measure the time evolution of pO_2 in mice using the exponential model of pO_2 decay. Previous studies have shown the feasibility of using a linear model of pO_2 decay during short breath-hold periods in humans and various animals (pigs, rabbits and guinea pigs). For humans, the period of linear decrease in pO_2 can be as long as 40 s (16). However, the length of this period depends on the metabolic rate per unit mass (29), and for mice it is expected to last only up to 4 s. Therefore, to be able to follow the time evolution of pO_2 accurately, it is necessary to use the nonlinear O_2 concentration decay model and to shorten the imaging time. The relevance of using the exponential pO_2 decay

DOI: 10.1002/nbm

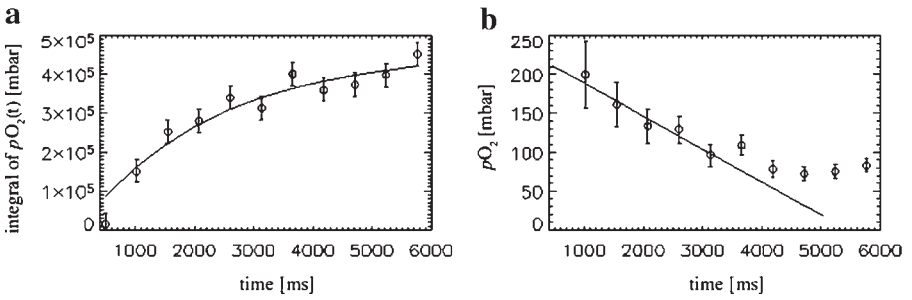

Figure 7. Example of the temporal evolution of the integral of pO_2*in vivo* for insufflation with ^{3}He/air mixture (ROI size = 1.6 mm^2) (a). For comparison, a corresponding plot was obtained using the linear approach (b).

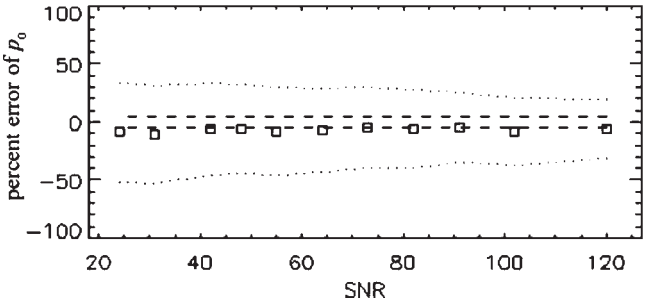

Figure 8. Percentage error of the mean measured p_0 value as a function of SNR. The dashed lines correspond to the +5% and −5% error of the simulated value. The dotted lines show the standard deviation of each measured p_0 value.

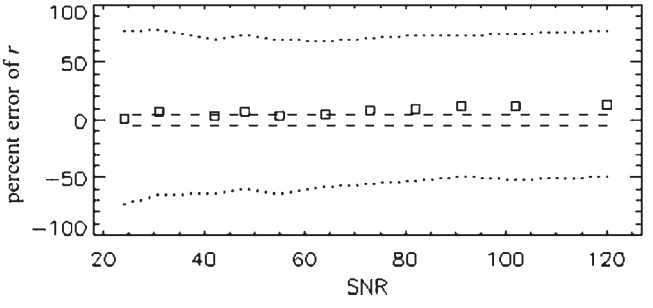

Figure 9. Percentage error of the mean measured r value as a function of SNR. The dashed lines correspond to the +5% and −5% error of the simulated value. The dotted lines show the standard deviation of each measured r value.

model is illustrated in Fig. 7, where use of both the linear and nonlinear approach for the same ROI is compared. The spiral acquisition scheme proposed in this work enables a series of images required for pO_2 measurement to be obtained in less than 6 s, making it suitable for imaging of mouse lungs during breath-hold. This time can be further reduced by acquiring fewer images in the series or by reducing the number of spirals per image.

The pO_2-sensitive method was validated *in vitro* for different gas mixtures, showing close agreement of the measured p_0 values with the predefined ones. The non-zero p_0 value measured in the syringe filled with pure ^{3}He can be explained by the dead volume of the valve. The pO_2 of 12 mbar is equivalent to an oxygen volume of about 0.06 ml, corresponding to 0.28 ml air, in conformance with the estimated dead volume of approximately 0.25 ml. Comparison of the estimated and measured p_0 values shows that the measurement technique may slightly underestimate the true p_0, in conformance with the simulation results (Fig. 8).

The *in vivo* experiments were conducted with two different gas compositions: pure ^{3}He and ^{3}He/air mixture. The following assumptions were made to estimate the p_0 values shown in Table 1: (1) the FRC of mouse lungs was about 0.5 ml (30); (2) the oxygen concentration in the FRC was approximately 15% (32): (3) the estimated dead volume of the tracheotomy tube and the valve was 0.27 ml. According to West (32), the partial pressure of dry gas in the lungs can be computed in the following way:

$$p_0 = [O_2][p_{ATM} - p(T)] \quad (7)$$

where $[O_2]$ denotes volume percentage of oxygen, p_{ATM} is the ambient pressure, and $p(T)$ is the water vapor pressure depending on temperature [$p(T) = 62.66$ mbar at body temperature]. As the lungs were insufflated at about 20 cm H_2O above atmospheric pressure (19.61 mbar), the final equation used to estimate p_0 was:

$$p_0 = [O_2](1013.25 + 19.61 - 62.66) \approx 970[O_2] \quad (8)$$

The oxygen concentration was calculated from the known gas volumes including the oxygen content in the FRC. The uncertainties of the estimated p_0 values take account of the mixing precision and the dead volume.

The pure ^{3}He insufflation resulted in the mean measured p_0 value of 77 ± 9 mbar, and the mean measured p_0 value for the mixture of air and ^{3}He was 107 ± 5 mbar (Table 1). In the case of both mixture compositions, the p_0 values obtained are in conformance with physiology (32).

The values of the depletion rate time constant were found to be in the range 6.0–8.3 s. To be able to compare the values of r with literature data on oxygen consumption in mice, the linear depletion rate R was estimated.

DOI: 10.1002/nbm

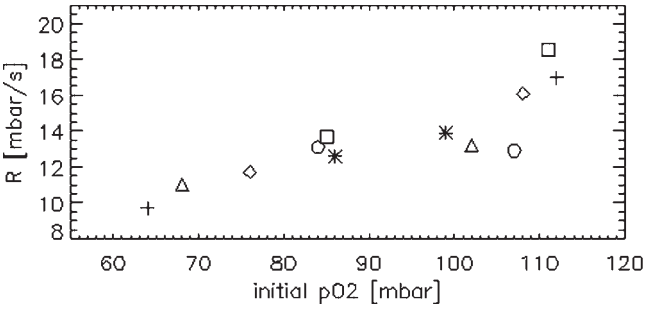

Figure 10. Correlation plot for p_0 and $R = p_0/r$. The linear Pearson correlation coefficient was 0.85. Symbols correspond to different animals: +, mouse 1; *, mouse 2; open circle, mouse 3; open diamond, mouse 4; open triangle, mouse 5; open square, mouse 6.

Expanding eqn (4) in the Taylor series gives:

$$pO_2(t) = p_0 \exp(-t/r) = p_0(1 - t/r + \ldots) = p_0 - (p_0/r)t + \ldots = p_0 - Rt + \ldots \quad (9)$$

The mean values of $R = p_0/r$ were computed for each animal and each insufflation. The literature values for the rate of oxygen consumption are 0.5–1.1 ml/min (30,31) for a mean body weight of 24 g, corresponding to about 6–15 mbar/s. The values found in the experiment are in agreement with these reference values except for two cases, which were slightly out of this range.

The rate of oxygen consumption is expected to be proportional to pO_2(16). As shown in Fig. 10, a positive linear correlation coefficient of 0.85 is observed between p_0 and R. This relationship reflects the match between oxygen depletion rate and pO_2 gradient between the alveolus and capillary blood.

The dispersion of the p_0 and r parameters is quite high (reaching 50% for the whole map). This high variability is in agreement with the simulation results, providing evidence that it is related to the inherent measurement errors. Nevertheless, it is comparable to the dispersion of the previously reported results of pO_2 mapping using ^{3}He-MRI (13) as well as other modalities (33–37). Hence, the inhomogeneity of the p_0 and r maps may also reflect the physiological conditions in the lungs. In view of the low precision of the measurement technique, parameters calculated as means over large ROIs seem to be more appropriate for estimating ventilation and perfusion in mouse lungs.

CONCLUSIONS

This study demonstrates the possibility of assessing alveolar pO_2 in mouse models using hyperpolarized ^{3}He. The time evolution of pO_2 was measured using a new approach assuming a nonlinear O_2 concentration decay model. Parametric maps of initial pO_2 and depletion rate time constant, r, were obtained with in-plane resolution of 1.6 mm^2. The results of this work show the relevance of using a nonlinear pO_2 decay model when imaging time and O_2 depletion time constant are comparable.

Acknowledgments

We acknowledge the financial support from the French CNRS-CEA ''Small Animal Imaging'' Program, and an MIRA grant from the Rhône-Alpes Region.

REFERENCES

1. Jalali A, Ishii M, Edvinsson JM, Guan L, Itkin M, Lipson DA, Baumgardner JE, Rizi RR. Detection of simulated pulmonary embolism in a porcine model using hyperpolarized ^{3}He MRI. *Magn. Reson. Med.* 2004; **51**: 291–298.
2. Rizi RR, Baumgardner JE, Ishii M, Spector ZZ, Edvinsson JM, Jalali A, Yu J, Itkin M, Lipson DA, Gefter W. Determination of regional V/Q by hyperpolarized ^{3}He MRI. *Magn. Reson. Med.* 2004; **52**: 65–72.
3. Gast KK, Beidermann A, Herweling A, Lehmann F, Schreiber WG, Schmiedeskamp J, Mayer E, Heussel C-P, Kauczor H-U, Eberle B. Oxygen-sensitive ^{3}He-MRI: intrapulmonary oxygen partial pressure and its distribution in lung transplant recipients. *Proc. Int. Soc. Magn. Reson. Med.* 2005; **13**: 1819.
4. Lipson D, Yu JS, Rajaei S, Emami K, Kadlecek S, Ishii M, MacDuffie Woodburn J, Hammond F, Vahdat V, Gefter W, Rizi RR. Differentiation of vasculopathy from normal pulmonary vasculature using hyperpolarized helium-3 MRI in humans. *Proc. Int. Soc. Magn. Reson. Med.* 2006; **14**: 39.
5. Miller GW, de Lange EE, Mata JF, Cai J, Cates GD, Tobias WA, Mugler JP III.Short-breath-hold pO_2 imaging with ^{3}He: initial experience in lung disease. *Proc. Int. Soc. Magn. Reson. Med.* 2006; **14**: 1289.
6. Deninger AJ, Eberle B, Ebert M, Großmann T, Heil W, Kauczor H-U, Lauer L, Markstaller K, Otten E, Schmiedeskamp J, Schreiber W, Surkau R, Thelen M, Weiler N. Quantification of regional intrapulmonary oxygen partial pressure evolution during apnea by ^{3}He MRI. *J. Magn. Reson.* 1999; **141**: 207–216.
7. Eberle B, Weiler N, Markstaller K, Kauczor H-U, Deninger A, Ebert M, Großmann T, Heil W, Lauer LO, Roberts TPL, Schreiber WG, Surkau R, Dick WF, Otten EW, Thelen M. Analysis of intrapulmonary O2 concentration by MR imaging of inhaled hyperpolarized ^{3}He. *J. Appl. Physiol.* 1999; **87**(6): 2043–2052.
8. Markstaller K, Eberle B, Schreiber WG, Weiler N, Thelen M, Kauczor H-U. Flip angle considerations in ^{3}He-MRI. *NMR Biomed.* 2000; **13**: 190–193.
9. Hedlund LW, Möller HE, Josette Chen X, Chawla MS, Cofer GP, Johnson GA. Mixing oxygen with hyperpolarized ^{3}He for small-animal lung studies. *NMR Biomed.* 2000; **13**: 202–206.
10. Möller HE, Hedlund LW, Josette Chen X, Carey MR, Chawla MS, Wheeler CT, Johnson GA. Measurements of hyperpolarized gas properties in the lung. Part III: ^{3}He T1. *Magn. Reson. Med.* 2001; **45**: 421–430.
11. Roberts D, Rizi R, Lipson DA, Hansen-Flaschen J, Yamamoto A, Gefter WB, Leigh JS, Schnall MD. Functional nonspecificity of T1-weighted MRI of laser-polarized ^{3}He gas. *Proc. Int. Soc. Magn. Reson. Med.* 2001; **9**: 946.
12. Olsson LE, Magnusson P, Deninger A, Pettersson G, Åkeson P, Petersson S, Golman K. Intrapulmonary pO_2 measured by low field MR imaging of hyperpolarized ^{3}He. *Proc. Int. Soc. Magn. Reson. Med.* 2002; **10**: 2021.
13. Fischer MC, Spector ZZ, Ishii M, Yu J, Emami K, Itkin M, Rizi R. Single-acquisition sequence for the measurement of oxygen partial pressure by hyperpolarized gas MRI. *Magn Reson Med.* 2004; **52**: 766–773.

DOI: 10.1002/nbm

14. Yu J, Fischer MC, Ishii M, Emami K, Vahdat V, Kadlecek S, Rizi RR. Measurements of regional alveolar oxygen pressure and oxygen depletion rate by hyperpolarized ^{3}He MRI in small animals. *Proc. Int. Soc. Magn. Reson. Med.* 2005; **13**: 1830.
15. Yu JS, Ishii M, Kadlecek S, MacDuffie Woodburn J, Emami K, Rajaei S, Hammond F, Vahdat V, Gefter W, Lipson D, Clark TWI, Brainard BM, Cheatham LR, Rizi RR. Simultaneous measurement of regional alveolar oxygen pressure, oxygen depletion rate and apparent diffusion coefficient by hyperpolarized ^{3}He MRI. *Proc. Int. Soc. Magn. Reson. Med.* 2006; **14**: 868.
16. Deninger AJ, Eberle B, Ebert M, Großmann T, Hanisch G, Heil W, Kauczor H-U, Markstaller K, Otten E, Schreiber W, Surkau R, Weiler N. ^{3}He-MRI-based measurements of intrapulmonary pO_2 and its time course during apnea in healthy volunteers: first results, reproducibility, and technical limitations. *NMR Biomed.* 2000; **13**: 194–201.
17. Deninger AJ, Eberle B, Bermuth J, Escat B, Markstaller K, Schmiedeskamp J, Schreiber WG, Surkau R, Otten E, Kauczor H-U. Assessment of a single-acquisition imaging sequence for oxygen-sensitive ^{3}He. *Magn. Reson. Med.* 2002; **47**: 105–114.
18. Wild J, Teh K, Woodhouse N, Ireland R, Fichele S, van Beek E, Paley M. Single scan 3D pO_2 mapping with hyperpolarized ^{3}He MRI. *Proc. Int. Soc. Magn. Reson. Med.* 2006; **14**: 869.
19. Lai Y-L, Hildebrandt J. Respiratory mechanics in the anesthetized rat. *J. Appl. Physiol.* 1978; **45**(2): 255–260.
20. Viallon M, Berthezène Y, Callot V, Bourgeois M, Humblot H, Briguet A, Crémillieux Y. Dynamic imaging of hyperpolarized ^{3}He distribution in rat lungs using interleaved-spiral scans. *NMR Biomed.* 2000; **13**: 207–213.
21. Riederer SJ, Tasciyan T, Farzaneh F, Lee JN, Wright RC, Herfkens RJ. MR fluoroscopy: technical feasibility. *Magn. Reson. Med.* 1988; **8**: 1–15.
22. Kerr AB, Pauly JM, Hu BS, Li KC, Hardy CJ, Meyer CH, Macovski A, Nishimura DG. Real-time interactive MRI on a conventional scanner. *Magn. Reson. Med.* 1997; **38**: 355–367.
23. Wagshul ME, Chupp TE. Optical pumping of high density Rb with a broadband dye laser and GaAlAs diode laser arrays: application to ^{3}He polarization. *Phys. Rev. A* 1989; **40**(8): 4447–4454.
24. Stupar V, Berthezène Y, Canet E, Tournier H, Dupuich D, Crémillieux Y. Helium3 polarization using spin exchange technique: application to simultaneous pulmonary ventilation/perfusion imaging in small animals. *Invest. Radiol.* 2003; **38**(6): 334–340.
25. O'Sullivan J. A fast sinc function gridding algorithm for Fourier inversion in computed tomography. *IEEE Trans. Med. Imag.* 1985; **MI-4**(4): 200–207.
26. Jackson J, Meyer CH, Nishimura DG, Macovski A. Selection of a convolution function for Fourier inversion using gridding. *IEEE Trans. Med. Imag.* 1991; **10**(1): 473–478.
27. Gudbjartsson H, Patz S. The Rician distribution of noisy MRI data. *Magn. Reson. Med.* 1995; **34**: 910–914.
28. Saam B, Happer W, Middleton H. Nuclear relaxation of ^{3}He in the presence of O_2. *Phys. Rev. A* 1995; **52**: 862–865.
29. Wilkinson MH, Berger PJ, Blanch N, Brodecky V. Effect of venous oxygenation on arterial desaturation rate during repetitive apneas in lambs. *Respir. Physiol.* 1995; **101**: 321–331.
30. Stahl WR. Scaling of respiratory variables in mammals. *J. Appl. Physiol.* 1967; **22**(3): 453–460.
31. Massaro GD, Mortola JP, Massaro D. Sexual dimorphism in the architecture of the lung's gas-exchange region. *Proc. Natl. Acad. Sci. USA* 1995; **92**: 1105–1107.
32. West JB. *Respiratory Physiology: The Essentials* (6th edition). Lippincott Williams & Wilkins: Baltimore, 1999.
33. Venegas JG, Galletti GG. Low-pass filtering, a new method of fractal analysis: application to PET images of pulmonary blood flow. *J Appl Physiol.* 2000; **88**: 1365–1373.
34. Musch G, Layfield JDH, Harris RS, Vidal Melo MF, Winkler T, Callahan RJ, Fischman AJ, Venegas JG. Topographical of distribution of pulmonary perfusion and ventilation, assessed by PET in supine and prone humans. *J Appl Physiol.* 2002; **93**: 1841–1851.
35. Glenny RW, Bernard SL, Robertson HT. Pulmonary blood flow remains fractal down to the level of gas exchange. *J Appl Physiol.* 2000; **89**: 742–748.
36. Altemeier WA, McKinney S, Glenny RW. Fractal nature of regional ventilation distribution. *J Appl Physiol.* 2000; **88**: 1551–1557.
37. Kreck TC, Krueger MA, Altemeier WA, Sinclair SE, Robertson TH, Shade ED, Hildebrandt J, Lamm WJE, Frazer DA, Polissar NL, Hlastala MP. Determination of regional ventilation and perfusion in the lung using xenon and computed tomography. *J Appl Physiol.* 2001; **91**: 1741–1749.

DOI: 10.1002/nbm